

Interplay of chemotaxis and chemokinesis mechanisms in bacterial dynamics

Maria R. D'Orsogna¹, Marc Suchard², and Tom Chou²¹Department of Physics & Astronomy, University of California, Los Angeles, CA 90095-1547 and²Department of Biomathematics, University of California, Los Angeles, CA 90095-1766

(Dated: November 10, 2018)

Motivated by observations of the dynamics of *Myxococcus xanthus*, we present a self-interacting random walk model that describes the competition between chemokinesis and chemotaxis. Cells are constrained to move in one dimension, but release a chemical chemoattractant at a steady state. The bacteria senses the chemical that it produces. The probability of direction reversals is modeled as a function of both the absolute level of chemoattractant sensed directly under each cell as well as the gradient sensed across the length of the cell. If the chemical does not degrade or diffuse rapidly, the one dimensional trajectory depends on the entire past history of the trajectory. We derive the corresponding Fokker-Planck equations, use an iterative mean field approach that we solve numerically for short times, and perform extensive Monte-Carlo simulations of the model. Cell positional distributions and the associated moments are computed in this feedback system. Average drift and mean squared displacements are found. Crossover behavior among different diffusion regimes are found.

PACS numbers: 87.17-d, 87.17-Jj

I. INTRODUCTION

The dynamics and pattern formation of bacteria serve as paradigms in understanding many properties of multi-cellular interacting systems, such as collective behavior, self organization, evolution, and development [1, 2]. The characteristics of bacterial motility and aggregation depend on numerous biological and chemical parameters, which include light exposure, temperature, concentration of food or of other substances, and lead to the existence of many classes of cell motion. Since a bacterium cannot utilize electromagnetic or acoustic radiation to sense its environment, it must rely on physical contact and its motility may depend on the production, diffusion and degradation of a relevant set of sensed chemicals. These chemicals are called chemoattractants or chemorepellants if they attract or repel bacteria, respectively. Examples of chemoattractants include food - sugars and amino acids - whereas antibiotics, fatty acids or other noxious substances are chemorepellant.

A prototype and well studied example of bacterial motility is the run and tumble mechanism used by *Escherichia coli* in liquid environments. The specialized structures allowing for cellular motion are known as flagellae, spinning helical tails which extend from the cellular membrane into the surrounding environment: counter-clockwise rotation of the flagellar motor leads to a one-directional run whereas clockwise rotation causes tumbling along a random direction. During its run, an *E. coli* cell periodically senses for chemosensitive substances, and, by comparing concentration levels in new and old environments, adjusts its motion and its likelihood to tumble in a new, randomly chosen, direction [3, 4]. If the cell is moving in the direction of increasing attractant, for instance, the probability of tumbling is lowered, so that the run time and 'mean free path' length in this direction are increased. An *E. coli* cell, thus, compares

chemical concentrations at nearby points, so that its future motion is determined by a chemical gradient [5, 6] via the mechanism of *chemotaxis*.

Chemotaxis may occur in other non-aqueous systems, such as in colonies of the bacterium *Myxococcus xanthus* or of the eukaryote *Dictyostelium discoideum* (slime-mould) which crawl on agar plates [7]. The exact regulatory mechanism leading to the surface gliding of these rod-like and slow moving organisms is yet unknown, and responses to external stimuli appear to be more complex than in enteric bacteria such as *E. coli* [8]. The cells undergo chemotaxis, but lack, or show very modest, responses to specific nutrient stimuli [9, 10], suggesting that the chemotactic behavior is due mainly to self-generated signaling chemicals [11]. The fact that cell density regulates typical reversal frequencies may be a consequence of one bacteria sensing the higher levels of signaling chemical in the presence of others [12]. In particular, under starving conditions, the cells are driven by auto-released fibril trails to aggregate and form multi-cellular compounds called fruiting bodies. These compounds raise above the agar plate and eventually sporulate into new and more resistant organisms which are then released to the environment in search of new sources of nutrients.

One major difference between these systems and enteric bacteria is that the chemoattractants embedded in or self-deposited on the agar plates are relatively immobile on the time scale of bacterial motility, whereas chemoattractant substances in aqueous environments have a finite diffusion constant. Like *E. coli*, the gliding cells can only sense what they come into immediate contact with, and since the chemosensitive substance diffuses slowly, large fibril concentration differences exist over the length of the cell. The gradient driving the chemotaxis mechanism is then determined between positions within a cell body length, as opposed to the large distances in-

volved in enteric bacteria chemotaxis.

Another possible mechanism driving cellular motility is *chemokinesis*. Here, changes in the direction of motion or in the cell velocity are determined locally, without recourse to the determination of concentration gradients. Chemokinesis may be a function of temperature, substrate adhesion, salt concentration or substances affecting the internal metabolism of the cell, slowing or enhancing its motion or turning frequency [13].

The observed patterns of movement of *M. xanthus* and of slime-mould suggest that the motility of these systems may be affected by self-induced chemokinesis as well as self-induced chemotaxis. *M. xanthus* move by shooting out and retracting pili from the ends of their prolate bodies [14, 15]. In nutritionally abundant environments or under conditions of high population density, both cellular systems generate repulsive fibril trails, leading to cell dispersion and the colonization of new regions of the agar plate. The mechanism is hypothesized to be dictated by chemokinesis [16, 17].

Previous theoretical studies into the collective dynamics of interacting motile bacteria, both of *E. coli* and *M. xanthus* type, include coarse-grained convective-diffusive transport type models [18, 19, 20, 21, 22] and lattice-type simulations [23, 24, 25]. These studies have considered the effects of interactions with concentration fields, modeling chemotaxis or chemokinesis or, as in Ref. [26], both chemosensitive mechanisms. The continuum theories take into account turning rates, and changes in speed or direction of motion, however they generally ignore long time path history effects induced by the sensed chemicals. In these systems, the bias to the motion arises from an external, fixed stimulus and not a dynamical one. Similar studies - with a fixed external trail - have been presented in different contexts, such as the aggregation of ants due to chemotaxis [27]. Other authors [28] have presented systems in which the fibril trail that dictates the motion of the cells is determined over an extended area and is not sensed locally.

The aim of this paper is to model and disentangle the effects of *self-generated* chemotaxis and chemokinesis, acting individually or concurrently and under diverse attractant and repulsive conditions. In contrast to many of the previous studies, the chemical trail of our systems will emerge from the motion of the bacterial cells and evolve with the cellular motion itself. Observations of individual organism paths may be more revealing of cellular dynamics than multicellular ensembles, and we restrict our attention to the behavior of a single bacterium. Even if isolated, the dynamics of this single cell will be affected by its self-secreted fibril trail, and the resulting pattern will be that of a self-interacting random walker. We shall try to understand cellular motion by developing, and analytically solving, the equations of motion for an isolated *M. xanthus* cell under a mean-field approximation, and by means of simple Monte-Carlo simulations, incorporating chemotaxis and chemokinesis to various degrees. The underlying assumption of this paper is that

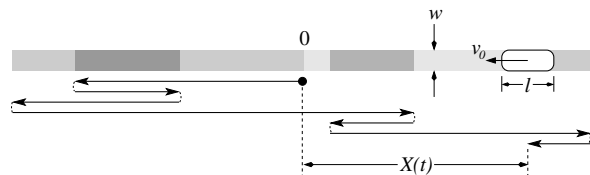


FIG. 1: The trajectory of a single bacterium of width w and length ℓ crawling in one dimension and depositing chemoattractant (or repellent) on the surface. The density of shading of the footprint is proportional to the total attractant deposited and arises from the hypothetical trajectory depicted by the arrows beneath. For the sake of simplicity, we have neglected the cell length ℓ in the depiction of the trajectory.

the chemosensitive material acts as a regulator of cell motion affecting only the frequency of direction reversal, via chemokinesis or chemotaxis. The speed of the bacterium is assumed constant in either direction and is controlled by inherent cellular bio-energetics.

Experimental single cell trajectories show that an isolated cell travels along its axis, occasionally veering off, and for the sake of simplicity, we will only consider one-dimensional dynamics. In order to validate our models, cell particle tracking can be eventually performed in one-dimensional etchings or imprints into the agar plates.

II. CONSTANT REVERSAL RATES

In this Section we derive a general Fokker-Planck equation for the single one-dimensional random walker. As discussed in the Introduction, we assume that the 'bacterium', or particle, travels with constant speed v_0 , and is subject to an *ad hoc* directional reverse mechanism that incorporates both chemotaxis and chemokinesis. To start, we ignore the effect of both phenomena, and we simply investigate the role of a constant reversal rate.

The probability that a bacterium is centered at position x at time t with velocity $\pm v_0$ will be denoted by $P_{\pm}(x, t)$ and the probability of a directional switch in time dt is $dt/\tau = \gamma dt$. If γ is independent of (x, t) we can write:

$$P_+(x, t) = P_+(x - v_0 dt, t - dt)(1 - \gamma_+ dt) + P_-(x, t)\gamma_- dt, \quad (1)$$

$$P_-(x, t) = P_-(x + v_0 dt, t - dt)(1 - \gamma_- dt) + P_+(x, t)\gamma_+ dt. \quad (2)$$

In the above equations, we have included the possibility that γ depends on the type of reversal, since in general the reversal rates from one direction to the other are not the same. Specifically:

$$\gamma_+ : +v_0 \rightarrow -v_0, \quad \gamma_- : -v_0 \rightarrow +v_0. \quad (3)$$

Expanding Eqns. (1) and (2) and keeping only the $O(dt)$ terms, we find:

$$\dot{P}_+(x, t) + v_0 \partial_x P_+(x, t) = -\gamma_+ P_+(x, t) + \gamma_- P_-(x, t), \quad (4)$$

$$\dot{P}_-(x, t) - v_0 \partial_x P_-(x, t) = -\gamma_- P_-(x, t) + \gamma_+ P_+(x, t). \quad (5)$$

The initial conditions are chosen so that at $t = 0$ the particle is localized at $x = 0$ with amplitudes a_{\pm} satisfying the condition that $a_+ + a_- = 1$:

$$P_+(x, 0) = a_+ \delta(x), \quad P_-(x, 0) = a_- \delta(x), \quad (6)$$

We obtain:

$$P_+(x, t) = \exp \left[\frac{(q_- x - q_+ v_0 t)}{2v_0} \right] \quad (7)$$

$$\left\{ \frac{a_+}{2} [\delta(x - v_0 t) + \delta(x + v_0 t)] + \Theta[v_0 t - |x|] \left[\frac{a_+ Q q_+}{4v_0} \sqrt{\frac{v_0 t + x}{v_0 t - x}} I_1 \left(\frac{q_+ Q}{2v_0} \sqrt{(v_0 t)^2 - x^2} \right) + \frac{a_- \gamma_-}{2v_0} I_0 \left(\frac{q_+ Q}{2v_0} \sqrt{(v_0 t)^2 - x^2} \right) \right] \right\};$$

$$P_-(x, t) = \exp \left[\frac{(q_- x - q_+ v_0 t)}{2v_0} \right] \quad (8)$$

$$\left\{ \frac{a_-}{2} [\delta(x - v_0 t) + \delta(x + v_0 t)] + \Theta[v_0 t - |x|] \left[\frac{a_- Q q_+}{4v_0} \sqrt{\frac{v_0 t - x}{v_0 t + x}} I_1 \left(\frac{q_+ Q}{2v_0} \sqrt{(v_0 t)^2 - x^2} \right) + \frac{a_+ \gamma_+}{2v_0} I_0 \left(\frac{q_+ Q}{2v_0} \sqrt{(v_0 t)^2 - x^2} \right) \right] \right\}.$$

Here, the parameters q_+ , q_- and Q are defined so that $q_+ = (\gamma_+ + \gamma_-)$, $q_- = (\gamma_- - \gamma_+)$ and $(q_+ Q)^2 = (q_+^2 - q_-^2)$. The function Θ is the Heaviside function, $\Theta(x)=1$ if $x > 0$, and the I functions are modified Bessel functions. The δ function terms carry the probability of the random walker cell having performed no reversals, and the Heaviside terms embody causality.

The total particle probability distribution function is $P(x, t) = P_+(x, t) + P_-(x, t)$. Under the symmetric condition $a_+ = a_- = 1/2$, and $\gamma_+ = \gamma_-$ (or equivalently $q_- = 0$) the solution reduces to that for the generalized Smoluchowski diffusion equation determined by Hemmer [29], which at large times is a spreading Gaussian. The Fourier transform of the distribution functions yields the moments of the random walker cell from which the cumulants can be extracted.

III. CHEMOKINESIS AND CHEMOTAXIS

We now consider the generation and sensing of chemoattractant or chemorepellant, and its effect on the reversal rates γ_{\pm} . *M. xanthus* cells deposit attractant

chemical matter contained within a fibril slime under the area of cell contact. We assume that the release of the chemoattractant occurs at a constant rate and uniformly over the cell-substrate footprint. In general, for a cell of length ℓ , the fibril concentration $\phi(x, t)$ obeys the following equation:

$$\dot{\phi}(x, t) = D \nabla^2 \phi(x, t) + r \Theta[\ell/2 - |x - X(t)|] - r_d \phi(x, t), \quad (9)$$

where the chemical is generated at a constant rate r per unit area. The Heaviside function Θ in Eq. (9) limits the increase in fibril concentration to the region strictly under the footprint of the bacterium centered at $X(t)$, whereas degradation and diffusion are included via the terms proportional to r_d and D . If the surface-deposited chemoattractant does not diffuse appreciably and $D \nabla^2 \phi$ is neglected, we find:

$$\phi(x, t) = \phi(x, 0) e^{-r_d t} + r \int_0^t dt' e^{r_d(t'-t)} \Theta[\ell/2 - |x - X(t')|]. \quad (10)$$

Note that $\phi(x, t)$ depends on the entire history of the trajectory $X(t')$ up to time $t' = t$. To couple the fibril concentration with cell dynamics, we must now include a relation between $\gamma_{\pm}(x, t)$ and $\phi(x, t)$. This relationship will depend on the particular mechanism of cell direction reversal and various choices will be discussed in the following subsections. It is important to note that, since we are assuming that fibril sensing is the main factor in determining direction reversals, we are also implicitly assuming that the sensing process, for example via a biochemical network within the bacterium, is much faster than the typical time for a cell to have moved appreciably. If we further take the molecular sensing apparatus to be distributed uniformly at the cell substrate footprint, the total chemoattractant $\Phi(X(t), t)$ sensed at time t is just the local contribution integrated over the cellular length:

$$\Phi(X(t), t) = w \int_{X(t)-\ell/2}^{X(t)+\ell/2} \phi(x, t) dx, \quad (11)$$

where w is the width of the cell as depicted in Fig. 1.

A. Chemokinesis

Let us consider the case of chemokinesis first. Here, the reversal rate depends only on the integrated fibril concentration. We will assume no intrinsic drift and set $\gamma(x, t) = \gamma_+(x, t) = \gamma_-(x, t)$. It is also reasonable to expect the switching probability to saturate for large enough fibril concentration, when the cell cannot respond to further increases in fibril levels. A plausible functional

dependence for γ on the total sensed chemoattractant Φ is of the type found in cooperative chemical binding, a Michaelis-Menten form with Hill coefficient β , so that for a cell at position $X(t) = x$, the reversal rate is:

$$\begin{aligned}\gamma(x, t) &= \gamma_0 + \kappa(x, t), \\ &= \gamma_0 + \delta p \frac{\Phi^\beta(x, t)}{\Phi_0^\beta + \Phi^\beta(x, t)},\end{aligned}\quad (12)$$

where Φ_0 and β , the inflection parameter and transition sharpness (or Hill coefficient), are peculiar to the system being considered. The effect of chemokinesis is measured by δp ; with the unbiased choice $\gamma_0 = 1/2$, δp is limited to $-1/2 \leq \delta p \leq 1/2$.

We must now solve Eqns. (4) and (5) with the above spatial and temporal dependence for $\gamma(x, t)$, which in turn depends on the concentration $\Phi(x, t)$ via Eqns. (10) and (11). The latter equations carry an explicit dependence on the past history of the walker. Our approach will be to consider the γ_0 contribution of Eq. (12) as giving rise to Eqns. (4) and (5) with constant reversal rates, and find its associated Green's function. The $\kappa(x, t)$ term in $\gamma(x, t)$ of Eq. (12) then generates non-homogeneous differential equations, whose solution may be obtained via the known Green's function. We will then be able to construct an iterative process to obtain $P(x, t)$ as a function of all preceding probabilities $P(x', t' < t)$. To build the Green's matrix function $\mathbf{G}(x, t)$, we note that Eqns. (4) and (5) can be written as:

$$\dot{\mathbf{P}}(x, t) = \mathbf{M}(x) \mathbf{P}(x, t), \quad (13)$$

where $\mathbf{P}(x, t) = [P_+(x, t), P_-(x, t)]^T$ and

$$\mathbf{M}(x) = \begin{pmatrix} -v_0 \partial_x - \gamma_+ & \gamma_- \\ \gamma_+ & v_0 \partial_x - \gamma_- \end{pmatrix}. \quad (14)$$

For the case of generic γ_\pm , independent of (x, t) , the solution to this equation, with the initial conditions expressed by Eqns. (6) is given by Eqns. (7) and (8). In the case $\gamma_+ = \gamma_- = \gamma_0$ we refer to these solutions as $P_+^{(0)}(x, t)$ and $P_-^{(0)}(x, t)$. The Green's function for this problem stems from the modified matrix equation:

$$\dot{\mathbf{G}}(x - x', t \geq 0) = \mathbf{M}(x) \mathbf{G}(x - x', t) + \mathbf{1} \delta(x - x') \delta(t), \quad (15)$$

$$\mathbf{G}(x - x', t < 0) = 0. \quad (16)$$

The fact that:

$$\mathbf{P}^{(0)}(x, t) = \begin{pmatrix} P_+^{(0)} \\ P_-^{(0)} \end{pmatrix}(x, t) = \mathbf{G}(x, t) \begin{pmatrix} a_+ \\ a_- \end{pmatrix}, \quad (17)$$

leads to the conclusion that the Green's matrix function is given by:

$$\mathbf{G}(x, t) = \begin{pmatrix} P_+^{(0)}(x, t)_{a_+=1} & P_+^{(0)}(x, t)_{a_+=0} \\ P_-^{(0)}(x, t)_{a_-=0} & P_-^{(0)}(x, t)_{a_-=1} \end{pmatrix}. \quad (18)$$

This result can also be verified by direct evaluation of $\mathbf{G}(k, \omega)$ in Fourier space. From Eqns. (4) and (5) it follows that reversal rates of the type $\gamma_\pm(x, t) = \gamma_0 + \kappa_\pm(x, t)$ yield a new matrix equation:

$$\dot{\mathbf{P}}(x, t) = \mathbf{M}(x) \mathbf{P}(x, t) + \mathbf{K}(x, t) \mathbf{P}(x, t). \quad (19)$$

where:

$$\mathbf{K}(x, t) = \begin{pmatrix} -\kappa_+(x, t) & \kappa_-(x, t) \\ \kappa_+(x, t) & -\kappa_-(x, t) \end{pmatrix}. \quad (20)$$

The resulting equation for $P(x, t)$ can be solved iteratively:

$$\begin{aligned}\mathbf{P}(x, t) &= \mathbf{P}^{(0)}(x, t) + \\ &\int_0^t dt' \int_{-\infty}^{\infty} dx' \mathbf{G}(x - x', t - t') \mathbf{K}(x', t') \mathbf{P}(x', t').\end{aligned}\quad (21)$$

In the case of chemokinesis, the non-homogeneous term $\kappa_+(x, t) = \kappa_-(x, t)$ is contained in Eq. (12). In order to simplify the expression for $\Phi(x, t)$, we assume unit cell width and take the limit of cellular length $\ell \rightarrow 0$. We also neglect diffusion and decay of the fibril. Under these assumptions, $\dot{\phi}(x, t) = r\ell\delta(x - X(t))$ and $\Phi(x, t) = w\ell\phi(x, t)$. The problem is now a deterministic one, as exemplified by the delta-function in the expression for $\dot{\phi}$. In order to apply Eq. (21), which gives the statistical probability for one bacterium to lie at (x, t) , we need to know its *exact* location at $X(t')$ for all previous times. In other words, the complete history of the cell is needed to determine future motion and solutions cannot be found.

Nevertheless, we can approximate $P_\pm(x, t)$ by an averaged density ρ_\pm , utilizing a mean field theory approach. Here, we average the probabilities P_\pm for a single walker over many distinct independent realizations, so that the self interaction is to be expressed on the *average* of all replicas of the system, and does not depend on the history of individual walkers. We can now rewrite the equation for the fibril concentration as:

$$\dot{\phi}(x, t) = r\ell\rho(x, t), \quad (22)$$

where we indicate the total bacterial density by $\rho(x, t)$. The above relationship signifies that, on average, fibril growth is proportional to the total density of bacteria at (x, t) . Integrating Eq. (22) and taking the initial condition $\phi(x, 0) = 0$, we obtain:

$$\phi(x, t) = r\ell \int_0^t dt' \rho(x, t'), \quad (23)$$

from which, using Eq. (21) and the definition $\Delta\rho(x, t) = \rho_+(x, t) - \rho_-(x, t)$ we can write:

$$\Delta\rho(x, t) = \Delta\rho^{(0)}(x, t) + \delta p \int_0^t dt' \int_{-\infty}^{\infty} dx' g(x - x', t - t') \frac{\Delta\rho(x', t') \phi^\beta(x', t')}{\phi_0^\beta + \phi^\beta(x', t')}. \quad (24)$$

Here $g(x, t)$ is a combination of the matrix elements of the Green's function: $g = -g_{11} + g_{12} + g_{21} - g_{22}$ and is even in x . An equation similar to Eq. (24) can be obtained for the total density $\rho(x, t)$, which depends on $\Delta\rho(x, t)$:

$$\rho(x, t) = \rho^{(0)}(x, t) + \delta p \int_0^t dt' \int_{-\infty}^{\infty} dx' h(x - x', t - t') \frac{\Delta\rho(x', t') \phi^\beta(x', t')}{\phi_0^\beta + \phi^\beta(x', t')}. \quad (25)$$

Here, $h = -g_{11} + g_{12} - g_{21} + g_{22}$ and is odd in x , as required by the normalization of both $\rho(x, t)$ and $\rho^{(0)}(x, t)$. It is useful to note that the above recursive equations may be used to evaluate the number density $n(x, t)$ for a system of N interacting bacteria as well. In this case, the distribution function $n_\pm(x, t) = N\rho_\pm(x, t)$ and the evolution equations are the same as (24) and (25) provided we redefine $\phi_0 = Nn_0$. Equations (23), (24) and (25) can now be solved numerically. Once $\Delta\rho(x, t)$ and $\rho(x, t)$ are determined, $\phi(x, t)$ can be evaluated and used to calculate the quantities of interest at subsequent times.

B. Chemotaxis

The incorporation of chemotaxis into the determination of the reversal rate follows closely that of chemokinesis. Let us consider chemotaxis as the sole reversal mechanism for a cell of length ℓ traveling at v_0 speed in the positive direction, and situated at position $X(t) = x$. The chemical gradient over the cellular length will drive the reversal rate. To specify the relation between gradient and reversal probabilities, we first introduce the probability terms $\mu_\pm(x, t)$:

$$\mu_\pm(x, t) = \exp \left[\mp \sigma \frac{\phi(x + \ell/2, t) - \phi(x - \ell/2, t)}{\ell} \right], \quad (26)$$

where σ is a constant that measures the strength of chemotaxis. For positive σ , the above expression translates into a low reversal probability whenever $\phi(x + \ell/2, t) > \phi(x - \ell/2, t)$ so that the cell is likely to keep moving speed at $+v_0$. This means we are modeling an attractant fibril trail. On the other hand, negative values of σ will represent a chemorepellant system. The same argument can be presented for a bacterium traveling at $-v_0$ speed. In this case, the direction of motion tends to persist for negative gradients, hence the expression for $\mu_-(x, t)$, where positive σ values signify chemoattractant

systems. In the limit of cellular length $\ell \rightarrow 0$, the above expressions are written as:

$$\mu_\pm(x, t) = \exp [\mp \sigma \phi_x(x, t)] \quad (27)$$

where the $\phi_x = \partial\phi/\partial x$. We use this exponential function to capture the sensitive chemical signalling, such as that found in *E. coli* [30]. Another alternative for the function μ_\pm is to include a saturation in the form of ϕ_x/ϕ in the exponent of (27).

We assume the reversal probabilities $\gamma_\pm(x, t)$ at position (x, t) to depend on $\mu_\pm(x, t)$ through the following:

$$\gamma_\pm(x, t) = \frac{1}{2} \left[1 + \frac{\mu_\pm(x, t) - 1}{\mu_\pm(x, t) + 1} \right], \quad (28)$$

so that for $\sigma = 0$, in the absence of chemotaxis, the reversal probabilities are $\gamma_\pm = \gamma_0 = \frac{1}{2}$.

We are now able to use the same formulation derived for the chemokinesis mechanism and apply it to the chemotactically driven case. Again, we must resort to the mean field calculation of the densities $\rho(x, t)$ and $\Delta\rho(x, t)$ by means of the Green's matrix function. The matrix \mathbf{K} appearing in the non-homogeneous term of Eq. (19) now has components $\kappa_\pm(x, t)$ given by:

$$\kappa_\pm(x, t) = \frac{\mu_\pm(x, t) - 1}{\mu_\pm(x, t) + 1}, \quad (29)$$

and Eq. (21) still holds. Note that since $\mu_-(x, t) = \mu_+^{-1}(x, t)$, then $\kappa_+(x, t) + \kappa_-(x, t) = 0$. Repeating the same type of calculations as for the chemokinesis case, for $\Delta\rho$ under chemotaxis we find:

$$\Delta\rho(x, t) = \Delta\rho^{(0)}(x, t) + \frac{1}{2} \int_0^t dt' \int_{-\infty}^{\infty} dx' g(x - x', t - t') \rho(x', t') \kappa_+(x', t'). \quad (30)$$

Here the previous history of the cell is contained in $\kappa_+(x', t')$ through the derivatives of the fibril concentration $\phi(x', t')$. The g function is the same as defined in the case of chemokinesis. Similarly, the density $\rho(x, t)$ is:

$$\rho(x, t) = \rho^{(0)}(x, t) + \frac{1}{2} \int_0^t dt' \int_{-\infty}^{\infty} dx' h(x - x', t - t') \rho(x', t') \kappa_+(x', t') \quad (31)$$

and $\rho(x, t)$ is properly normalized by the fact that $h(x, t)$ (defined in the previous subsection) is odd with respect to x .

C. Combined Chemokinesis and Chemotaxis

If the two mechanisms of chemokinesis and chemotaxis are active, both δp and σ are non-zero, and $\gamma_{\pm}(x, t)$ must include both contributions. For $\gamma_{\pm}(x, t)$, we write:

$$\gamma_{\pm}(x, t) = \frac{1}{2} \left\{ 1 + \frac{p_k(x, t)[\mu_{\pm}(x, t) + 1] - 1}{p_k(x, t)[\mu_{\pm}(x, t) - 1] + 1} \right\}. \quad (32)$$

Here, $p_k(x, t)$ is the contribution from chemokinesis in the form expressed by Eq. (12) with $\gamma_0 = 1/2$, i.e. $p_k(x, t) = \gamma(x, t)$ from the chemokinesis case. The contribution from chemotaxis is $\mu_{\pm}(x, t)$ as defined by Eq. (27).

The choice $\sigma = 0$ sets $\gamma_{\pm}(x, t) = p_k(x, t)$, that is, the rate is dictated only by the chemokinesis mechanism. Conversely, $\delta p = 0$ sets $p_k = 1/2$ and $\gamma_{\pm}(x, t)$ reduces to the purely chemotactic expressions of Eq. (28). For both $\sigma = \delta p = 0$ the reversal rate is $1/2$. The corresponding $\kappa_+(x, t)$ and $\kappa_-(x, t)$ are contained in Eq. (32) and yield the following recursive relationship for $\Delta\rho(x, t)$:

$$\Delta\rho(x, t) = \Delta\rho^{(0)}(x, t) + \int_0^t dt' \int_{-\infty}^{\infty} dx' g(x - x', t - t') \frac{1}{2} [\mathcal{U}(x', t')\rho(x', t') + \mathcal{V}(x', t')\Delta\rho(x', t')]. \quad (33)$$

The corresponding equation for $\rho(x, t)$ is:

$$\rho(x, t) = \rho^{(0)}(x, t) + \int_0^t dt' \int_{-\infty}^{\infty} dx' h(x - x', t - t') \frac{1}{2} [\mathcal{U}(x', t')\rho(x', t') + \mathcal{V}(x', t')\Delta\rho(x', t')]. \quad (34)$$

Here, the $\mathcal{U}(x, t)$ and $\mathcal{V}(x, t)$ functions depend on chemotaxis and chemokinesis via:

$$\mathcal{U} = \frac{p_k(1 - p_k)(1 - \mu_+^2)}{[p_k(\mu_+ - 1) + 1][\mu_+(p_k - 1) - p_k]}, \quad (35)$$

$$\mathcal{V} = \frac{\mu_+(1 - 2p_k)}{[p_k(\mu_+ - 1) + 1][\mu_+(p_k - 1) - p_k]}. \quad (36)$$

We have used $\mu_+\mu_- = 1$ and suppressed the (x, t) dependence. Note that in the absence of chemotaxis, for $\sigma = 0$ and $\mu_+ = 1$, $\mathcal{U} = 0$ and $\mathcal{V} = 2p_k - 1$, leading to the pure chemokinesis case. In the absence of chemokinesis, for $p_k = 1/2$, $\mathcal{U} = \kappa_+$, as defined in the previous subsection, and $\mathcal{V} = 0$. We shall discuss the numerical solution to the equations for $\rho(x, t)$ and $\Delta\rho(x, t)$ in the various cases of chemokinesis, chemotaxis or both, in the next Section.

IV. DISTRIBUTION FUNCTIONS

In this Section, by means of numerical integration, we solve equations (25), (24), (31), (30), (33), and (34) for

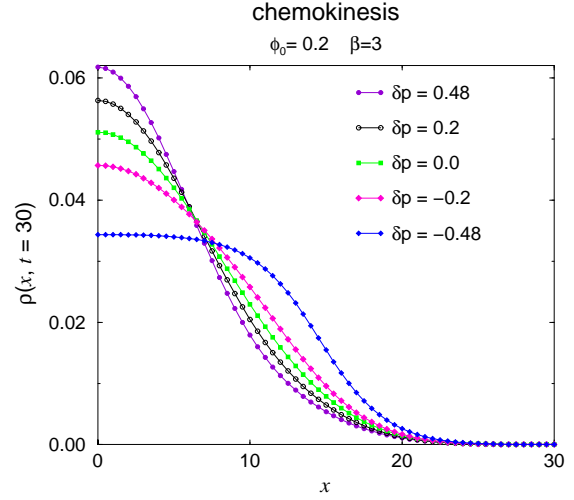


FIG. 2: Distribution functions in the case of chemokinesis for $\phi_0 = 0.02$ and $\beta = 3$. Note that $\delta p > 0$ increases the reversal rate, localizing the cell at the initial position and $\delta p < 0$ values have the opposite effect. The time scale is $n = 600$ time steps in units of $\Delta t = 0.05$.

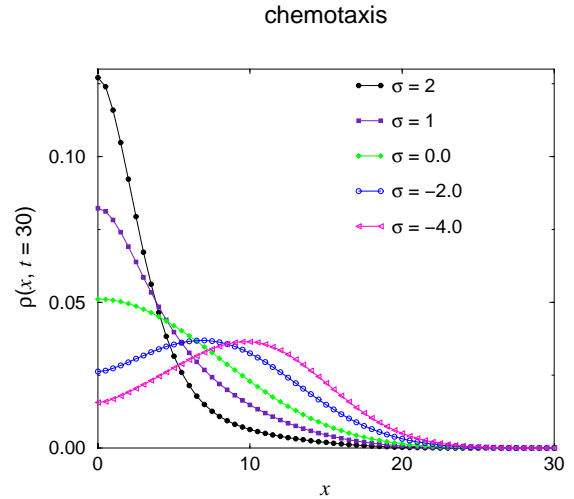


FIG. 3: Distribution functions in the case of chemotaxis for different σ values. Note that $\sigma > 0$ values represent chemoattraction and the cells are localized at the initial position, $\sigma < 0$ values instead represent chemorepulsion and two repelling opposite peaks develop. The time scale is $n = 600$ time steps in units of $\Delta t = 0.05$.

$\rho(x, t)$ and $\Delta\rho(x, t)$. Under chemokinesis, Eqns. (25) and (24) are Volterra equations of the second kind in the t variable, for which standard methods can be applied [31]. In particular, we discretize both the temporal and spatial axis according to a uniform mesh, of spacing Δt and Δx , and solve the two coupled equations iteratively.

Let us assume that $\Delta\rho(x', t' < t)$ and $\rho(x', t' < t)$ are known, where t' represent time steps up to $t - \Delta t$. At the subsequent time step t , $\Delta\rho(x, t)$ is evaluated by cal-

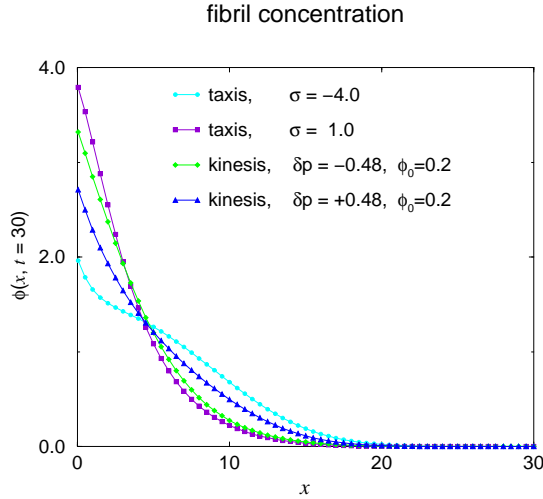


FIG. 4: Fibril concentration $\phi(x, t)$ in the case of either chemotaxis or chemokinesis for different σ and δp values. The time scale is $n = 600$ time steps in units of $\Delta t = 0.05$. In the chemokinesis curves $\phi_0 = 0.2$, close to the saturation limit of the Michaelis-Menten form of Eq. 12.

culating $\Delta\rho^{(0)}(x, t)$ and by adding to it the sum over all previous time steps $t' < t$ of the integrand. Of these terms, the last one, at $t = t'$, contains the kernel function $g(x - x', 0) = -2\delta(x - x')$, which, when integrated over space, extracts a term proportional to the quantity of interest, $\Delta\rho(x, t)$. The other contributions of the sum, for $t \neq t'$, are spatial integrals, that are evaluated as sums after the discretization over the x' variable. These sums contain the known values of $\Delta\rho(x', t' < t)$, as well as $\kappa(x', t')$ which depends on the fibril concentration $\phi(x', t')$. The latter is just the integrated $\rho(x', t')$ as follows from Eq. (23). In order to evaluate $\phi(x', t')$, a time discretized summation over the $\rho(x', t' < t)$ values is carried out. The assumption here is that the bacterium senses the environment before laying down new fibril, so that the concentration $\phi(x', t')$ is evaluated not by the trapezoidal rule, in which the extrema of the integration region are weighed each as 1/2, but by weighing $t = 0$ with 1 and ignoring $t = t'$. In the case of chemokinesis, once $\Delta\rho(x, t)$ is determined, $\rho(x, t)$, which depends on $\Delta\rho(x', t')$, can be calculated in the same way.

In Fig. 2 we plot the results for $\rho(x, t)$ for a system under chemokinesis. The meshes are set at $\Delta x = \Delta t = 0.05$ and the maximum time step, in these units is $t = 600$. Cell velocity is fixed at $v_0 = 1$ and the parameter $\phi_0 = 0.2$. For chemoattractant fibril, or $\delta p > 0$, the distribution is narrower than the bare $\delta p = 0$ case, also plotted in the graph. Negative values of δp represent chemorepulsion and broaden the distribution, eventually leading to a plateau-like region. The existence of the plateau is due to the fact that for large negative values of $\delta p \simeq -1/2$ the reversal rate at saturation is almost zero, leading to ballistic motion of the cell in the region where the fibril has been deposited. Once the cell reaches

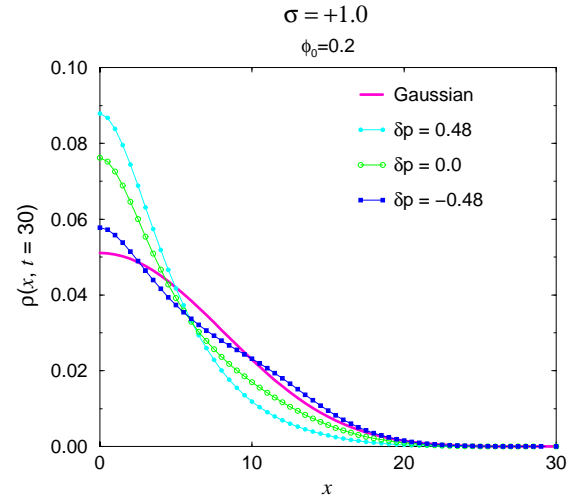


FIG. 5: Distribution functions under chemotaxis, set at $\sigma = +1.0$, and chemokinesis set at various δp values. The time scale is $n = 600$ time steps in units of $\Delta t = 0.05$.

the edge of the plateau region of fibril concentration, the reversal rate increases dramatically and the cell tends to reverse its motion and travel backwards, until the opposite side of the plateau region is reached. This behavior accounts for the uniformity of the distribution function in the central region. Time evolution also tends to broaden - and consequently lower - the plateau region, since the bacteria tend to build up fibril at the edges, thus increasing the range of motion.

For the case of chemotaxis, $\rho(x, t)$, is easier to evaluate, since it can be calculated without recourse to $\Delta\rho(x, t)$, as indicated by Eq. (31). The procedure is the same as that outlined for the case of chemokinesis. We take the gradient appearing in the expressions for μ_{\pm} to be evaluated over a distance $\ell = 2$, so that for $x = x_i$ and $t = t_i$ of the mesh we have:

$$\mu_{\pm}(x_i, t_j) = \exp \left[\mp \frac{\sigma}{2} [\phi(x_{i+1}, t_j) - \phi(x_{i-1}, t_j)] \right]. \quad (37)$$

Results are plotted in Fig.3. As discussed in the previous section, positive (negative) values of σ indicate chemoattraction (chemorepulsion). It is interesting to note that for large negative values of σ two peaks develop (only one is seen from Fig. 3, the other is its symmetrical image in the x axis), with the bacteria traveling towards unexplored regions of space, void of fibril.

When both mechanisms are present, chemotaxis and chemokinesis may enforce or compete against each other in their localizing or spreading effects. Chemoattractant values of $\sigma > 0$ for instance, contrast the ballistic tendency of $\delta p < 0$, and viceversa, chemorepulsive values of $\sigma < 0$ oppose the localizing effect of $\delta p > 0$. In Figures 5 through 7, we examine the interplay of the two mechanisms for several values of σ and δp .

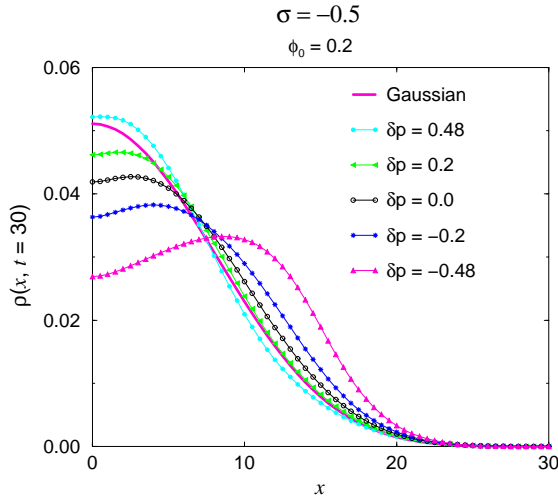


FIG. 6: Distribution functions under chemotaxis, set at $\sigma = -0.5$, and chemokinesis set at various δp values. The time scale is $n = 600$ time steps in units of $\Delta t = 0.05$.

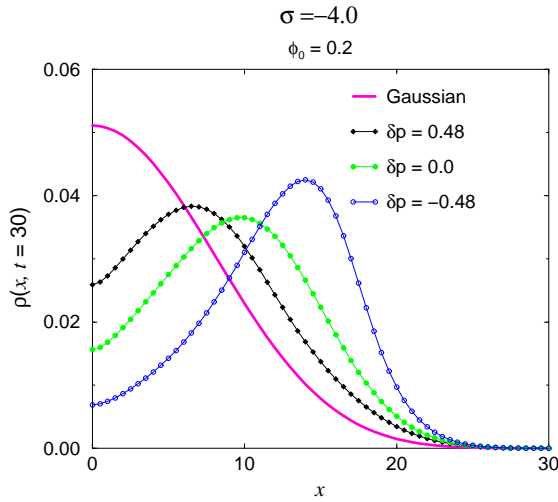


FIG. 7: Distribution functions under chemotaxis, set at $\sigma = -4.0$, and chemokinesis set at various δp values. The time scale is $n = 600$ time steps in units of $\Delta t = 0.05$.

For both $\sigma, \delta p > 0$ the distribution functions are localized about the central position, whereas for $\sigma, \delta p < 0$ two peaks traveling in opposite directions develop. The sharpness of these peaks increases with increasing $|\sigma|$, as can be seen by comparing Figures 6 through 7. and the localization position increases with increasing $|\delta p|$ as each figure also shows. Competing effects arise when δp and σ are of opposite signs. For large negative values of σ , the effect of positive δp values is simply to shift the mean of the spreading peak towards the origin (Figures 7). For smaller negative values of σ increasing δp tends to localize the distribution functions at the origin, until the

traveling peak is washed out and a plateau region, typical of large positive δp values forms (Fig. 6). Finally, in the regime of $\sigma > 0$ and $\delta p < 0$, the localizing tendency due to chemoattraction is offset by the chemokinesis-plateau tendency. Unusual distribution function patterns may arise as in the case of $\sigma = 0.5$ or $\sigma = 1$ and $\delta p = -0.4$ or $\delta p = -0.48$ in Fig. 5.

V. MONTE-CARLO SIMULATIONS

To analyze the statistics of the one dimensional dynamics of cell motion under chemotaxis and chemokinesis, we also implemented a stochastic simulation on a 1D lattice. We discretize space and time and assume the random walker cell to have finite length ℓ . At time $t = 0$, the single cell is positioned at the origin of a one dimensional track and there is no fibril substance present. Fibril is constantly secreted by the cell and the dynamics of the particle position obeys:

$$X_{t+1} = X_t + \eta_t(X_t - X_{t-1}), \quad (38)$$

where X_{t+1} is the position of the center of the cell at time $t + 1$ and $X_t - X_{t-1}$ indicates the direction it was traveling prior to time t . The stochastic random variable η_t is defined as:

$$\eta_t = \begin{cases} -1 & \text{with prob. } \gamma_t \\ +1 & \text{with prob. } 1 - \gamma_t \end{cases} \quad (39)$$

where γ_t is the probability for the cell to reverse its direction, before the time step at $t + 1$. The initial direction of motion is chosen so that X_{-1} is ± 1 with equal probability. We simultaneously model chemotaxis and chemokinesis through the dependence of γ_t on the self secreted fibril concentration $\phi(x, t)$, as in the continuum case. Discretizing equations (9) and (11) we obtain:

$$\phi_t(x) = \sum_{s=0}^t \Theta(\ell/2 - |x - X_s|), \quad \text{and} \quad (40)$$

$$\Phi_t(x) = \sum_{x=-\ell/2}^{\ell/2} \phi_t(X_t + x), \quad (41)$$

where $\phi_t(x)$ is the amount of chemoattractant that has built up at location x and Φ_t is the total amount of chemoattractant sensed by the cell. Both $\phi_t(x)$ and Φ_t naturally depend on the past trajectory of the cell, which we keep track of as the simulation proceeds. We let $p_{t,k}$ represent the probability of direction reversal based on chemokinesis alone derived from equation (12). This probability is then stretched towards 0 or 1 depending on the local normalized chemical gradient in chemotaxis,

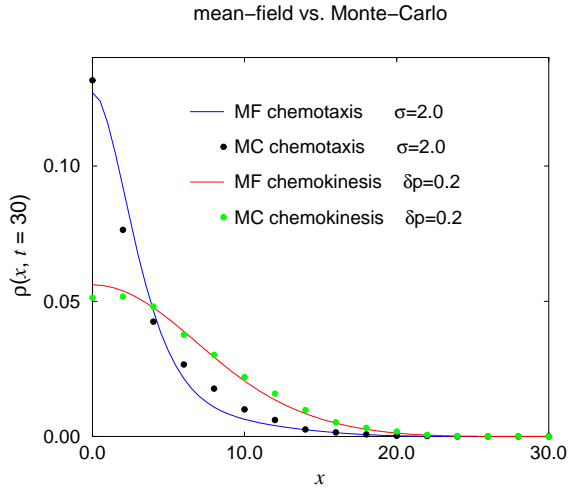


FIG. 8: Comparison of mean-field theory results with Monte-Carlo simulations for short times. The mean-field curves are evaluated after $n = 600$ time steps of $\Delta t = 0.05$ and the Monte-Carlo curves are determined after $t = 30$ time steps. In the chemokinesis Monte-Carlo curve $\Phi_0 = 4$, whereas in the chemokinesis mean-field curve $\phi_0 = 0.2$. The factor of 0.05 is needed to take into account the discretization of the numerical Volterra-type evaluation.

through the quantity $\mu_{t,c}$. Analogous to Eqs. (12) and (26) in the continuum theory, the kinesis and chemotaxis effects are represented by:

$$p_{t,k} = \frac{1}{2} + \delta p \frac{\Phi_t^\beta}{\Phi_0^\beta + \Phi_t^\beta}, \quad (42)$$

$$\mu_{t,c} = \exp[-\sigma(X_t - X_{t-1})\nabla\phi_t], \quad (43)$$

where $\nabla\phi_t = \phi_t(X_t + \ell/2) - \phi_t(X_t - \ell/2)$ and δp and σ are weight parameters subject to the constraints:

$$-\frac{1}{2} \leq \delta p \leq \frac{1}{2} \text{ and } -\infty < \sigma < \infty. \quad (44)$$

The parameter σ scales the effect size of chemotaxis, with no chemotaxis corresponding to $\sigma = 0$; while δp scales the strength of chemokinesis, with no chemokinesis corresponding to $\delta p = 0$. At each step of the Monte-Carlo iteration, the total reversal probability is calculated as:

$$\gamma_t = \frac{1}{2} \left[1 + \frac{p_{t,k}(\mu_{t,c} + 1) - 1}{p_{t,k}(\mu_{t,c} - 1) + 1} \right]. \quad (45)$$

In Fig. 8 we compare the results from the Monte Carlo simulations and the mean-field approximation of the previous section, for small times, for a typical case of chemokinesis and chemotaxis.

We can now analyze results of the Monte-Carlo simulations for longer times than in the analytic case: $t_{max} =$

10^5 . At these time scales, the general trends found in the analytic case persist for most combinations of $(\sigma, \delta p)$. The simulation results are summarized in a phase-diagram. Positive values of δp and σ both cause attractiveness in the system and we expect suppressed spreading of the distribution function. Negative values of δp and σ on the other hand cause repulsion and enhanced spreading. To quantify these effects, we compared the distribution function $P(x, t_{max})$ with a normalized Gaussian, corresponding to the parameters $\sigma = \delta p = 0$. More specifically, we compare the integral of the reference Gaussian at the curvature inflexion points to the integral of the probability distribution function between the same limits. If the integral of the PDF is less than that of the corresponding Gaussian, the dynamics is classified as being suppressed. This definition is shown in Fig. 9(top). We explore the entire phase space δp and σ and find the crossover from one regime to the other. The enhanced or suppressed diffusive character of the PDF curves may evolve from that of the early time regime, but it is found that after $t = 10^3$ simulation time steps the classification is stable. The phase diagram is shown in Fig. 9(bottom). For $\sigma, \delta p > 0$, both kinesis and chemotaxis effects suppress the diffusivity of the trajectories. Only for $\sigma < 0$ can the spreading dynamics be enhanced. Due to our choice of the functional forms of the effects (Eqs. 12 and 26), the dynamics are much more sensitive to σ than δp , nonetheless, the effects of kinesis induces an asymmetry in δp in the phase diagram. The curve approaches the limits $\delta p = \pm 0.5$ asymptotically.

VI. CONCLUSION

In this paper we presented a mean field model and Monte-Carlo simulations for bacterial dynamics under the mechanisms of chemokinesis and chemotaxis acting concurrently. The bacterial motion is that of a one-dimensional self-interacting random walker. The fibril trail that governs the dynamics of the system is itself a dynamical quantity that depends on the past motion of the cells. We model the two mechanisms in terms of two characterizing parameters, σ and δp , which represent, respectively, the degree of chemotaxis and chemokinesis. The mean-field results agree with Monte-Carlo simulations in the limit of short times. For long times we find a phase-diagram in $(\sigma - \delta p)$ space that separates enhanced or suppressed diffusion regimes. In contrast to the short-time numerics displayed in Figs. 2-7, which show PDFs indicative of enhanced diffusion for $\delta p < 0$, the long time phase diagram exhibits suppressed diffusion provided σ is negative and $|\delta p|$ is not too large. Therefore, in the long-time limit, kinesis modeled by the logistic saturation, Eq. (12), results in suppressed diffusion in the absence of chemorepellent effects ($\sigma < 0$). We have investigated the effects of increased cooperativity in the biochemical signaling through the β parameter. As can be seen from Fig. 9 increased β values do not significantly affect the

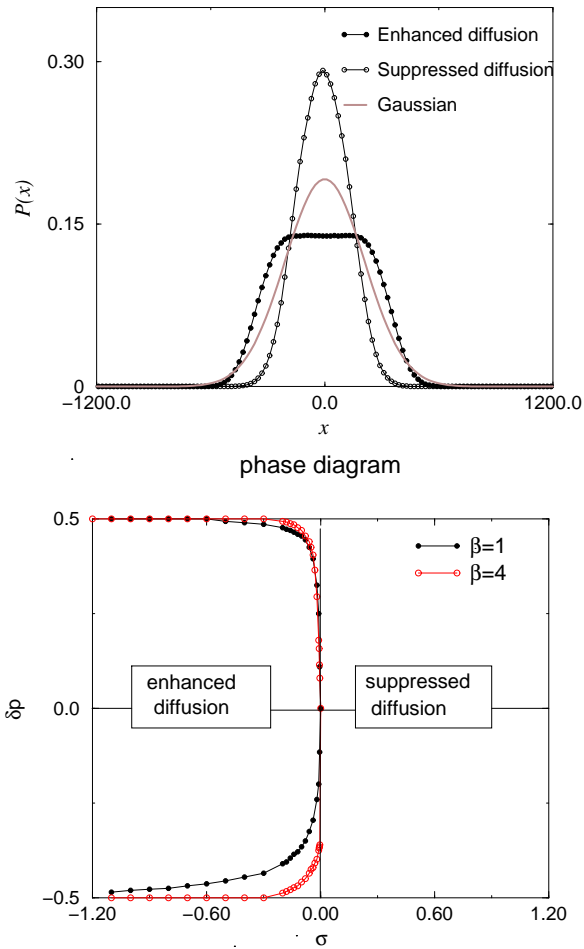


FIG. 9: (top) Gaussian and suppressed and enhanced PDFs. (bottom) $\sigma - \delta p$ phase diagram at $t = 10^5$ for $\beta = 1, 4$. The crossover between suppressed and enhanced diffusion was found by Monte-Carlo simulations and determining the point at which the integral of the reference Gaussian between the curvature inflexion points is equal to that of the distribution functions.

phase-diagram curve.

The model exhibits variations in shapes of the particle PDF. The characteristic PDF shapes depend on whether long or short time dynamics are considered.

One of the possible applications of this work is for isolated A-motility (adventurous) Myxobacteria cells whose dynamics is driven by self-secreted slime and does not require the presence of neighboring cells in direct contact [32, 33]. Our analysis is restricted to a one-dimensional system. For a single cell constrained to move along a 1D agar track, the relevant parameters (σ , δp and β) of our model can be tuned to identify the correct mechanism of motion. Moreover, the motion of freely moving A-type myxobacteria cells is *locally* one-dimensional. Our model

does not account for contact interactions between cells, rather, cells interact indirectly via trails of self-secreted slime. This simplification enables us to study the details of the effects of the history-dependent fibril concentration. Direct cell-cell signalling interactions on a 2D aggregating colony are known to lead to the formation of complex structures such as propagating rippling waves and spiraling fruiting bodies [10, 32]. Although the investigation of contact interactions between cells is beyond the scope of this paper, our approach does not preclude the formation of propagating waves and associated rippling patterns in systems where fibril-mediated cell-cell interactions are included.

The authors are grateful for the assistance of G. Lakatos in improving the implementation of our simulations and numerical computations. MD and TC were supported by the National Science Foundation through grant DMS-0206733.

- [1] T.M. Preston, C.A. King, and J.S. Hyams, *The cytoskeleton and Cell Motility*, (Blackie, Glasgow and London, 1990).
- [2] E. Ben-Jacob, I. Cohen and H. Levine *Adv. Phys.*, **49**, 395, (2000).
- [3] H.C. Berg and E.M. Purcell, *Biophys. J.*, **20**, 193, (1977).
- [4] D.E. Woodward, R. Tyson, M.R. Myerscough, J.D. Murray, E.O. Budrene, and H.C. Berg, *Biophys. J.* **68**, 218, (1989).
- [5] H. C. Berg and D. A. Brown, *Nature*, **239**, 500-504, (1972).
- [6] M. P. Brenner, L. S. Levitov and E. O. Budrene, *Biophys. J.* **74**, 1677, (1998).
- [7] D.B. Kearns and L.J. Shimkets, *PNAS* **95**, 11957, (1998).
- [8] W. J. Rappel, P. J. Thomas, H. Levine and W. F. Loomis *Biophys. J.* **83**, (2002).
- [9] W. Shi and D.B. Kearns, *Nature* **366**, 414, (1993).
- [10] S. Tieman, A. Koch and D.A. Kaiser, *J. Bacteriol.* **178**, 3480, (1996).
- [11] D.B. Kearns, A. Venot, P.J. Bonner, B. Stevens, G. Boons and L.J. Shimkets, *PNAS* **98**, 13990, (2001).
- [12] W. Shi, F. K. Ngok, and D. Zusman, *Proc. Natl. Acad. Sci.*, **93**, 4142-4146, (1996).
- [13] D. R. Soll *J. Chem. Ecol.*, **16**, 1, (1990).
- [14] A. M. Spormann, *Microbiol. Mol. Biol. Rev.* **63**, 621, (1999).
- [15] A. J. Merz, M. So, and M. P. Sheetz, *Nature*, **407**, 98-102, (2000).
- [16] M.J. Ward and D.R. Zusman *Mol. Microbiol.* **24**, 885, (1997).
- [17] M.J. Ward, K.C. Mok and D.R. Zusman *J. Bacteriol.* **180**, 440, (1998).
- [18] *J. Math. Biol.* **9**, 147-177, (1980).
- [19] E. F. Keller, *Antibiotics and Chemotherapy*, **19**, 79-93, (1974).
- [20] J. C. Dallon and H. G. Othmer, *J. Theor. Biol.*, **194**, 461-483, (1998).
- [21] E. Palsson and H. G. Othmer, *Proc. Natl. Acad. Sci.*, **97**, 1044810453, (2000).
- [22] R. Nossal, *Math. Biosci.*, **31**, 121-129, (1976).
- [23] H. G. Othmer and A. Stevens, *SIAM J. Appl. Math.*, **57**, 1044-1081, (1997).
- [24] H. G. Othmer and T. Hillen, *SIAM J. Appl. Math.*, **57**, 1044-1081, (1997).
- [25] A. Stevens, *J. Biol. Sys.*, **3**, 1059-1068, (1995).
- [26] T. Hillen, C. Rohde and F. Lutscher, *J. Math. Anal. Appl.*, **260**, 173, (2001).
- [27] D. Chowdhury, V. Guttal, K. Nishinari, A. Schadschneider, *J. Phys. A*, **L573**, (2002).
- [28] F. Cecconi, M. Marsili, J. R. Banavar and A. Maritan, *Phys. Rev. Lett.*, **89**, 2002.
- [29] P.C. Hemmer, *Physica* **27**, 79-82, (1961).
- [30] J. E. Segall, S. M. Block, and H. C. berg, *Proc. Natl. Acad. Sci.*, **83**, 8987-8991, (1986).
- [31] W.H. Press, S.A. Teukolosky, W.T. Vetterling and B.P. Flannery, *Numerical Recipes in C, Second Edition*, Chapter 18.2, (Cambridge University Press, Cambridge, 1999).
- [32] C. Wolgemuth, E. Hoiczyk, D. Kaiser and G. Oster, *Curr. Biol.* **12**, 369-377, (2002).
- [33] O. Igoshin and G. Oster, *Math. Biosci.* (in press)